Review Paper

International Journal of Research and Review
[Indexed, Peer-Reviewed Journal]
Volume 12; Issue: 3; March 2025
Website: www.ijrrjournal.com
E-ISSN: 2349-9788; P-ISSN: 2454-2237

Comprehensive Review of Sintered Silver Porous Structures and Their Thermal Aging for Power Device Packaging

Kokouvi Happy N'TSOUAGLO[1,2], Komlavi GOGOLI[2], Kodjo ATTIPOU[1,2]

[1]Department of Mechanical Engineering, Polytechnic School of Lomé, University of Lomé, Togo
[2]Laboratory of Structure and Mechanic of Materials LaS2M, University of Lomé, Lomé, Togo.

Corresponding Author: Kokouvi Happy N'TSOUAGLO

DOI: https://doi.org/10.52403/ijrr.20250325

ABSTRACT

Wide band gap (WBG) devices, using sintered silver (s-Ag) for die attachment are attracting increasing interest due to silver's excellent properties and its ability to operate at high temperatures. However, the sintering process results in a porous structure whose evolution during thermal aging is known to degrade the material's properties. This review article presents the conventional silver sintering process, critically analyzes the resulting porous microstructures based on various approaches, and examines the impact of thermal aging on microstructural evolution. It highlights the challenges associated with controlling this microstructure and offers perspectives for future research directions.

Keywords: Die-attach reliability, microstructural evolution, sintered Silver, thermal aging

1. INTRODUCTION

In recent years, advances in power electronics have driven the rise of electric and hybrid vehicles, fifth-generation (5G) technologies, and other energy conversion applications. These innovations address user comfort needs while reducing greenhouse gas emissions. However, they impose increasing technical requirements, particularly with the use of new semiconductors like silicon carbide (SiC), capable of operating at high temperatures of up to 350 °C [1], [2]. Simultaneously, the RoHS (Restriction of Hazardous Substances) directive has restricted the use of hazardous substances such as lead (Pb), a key component in traditional solders [3], [4], [5].

These technical and regulatory constraints call into question the relevance of conventional brazing alloys, such as those based on SnPb. These materials have low thermal conductivity and problems with creep and fatigue at high temperatures, limiting their reliability in severe thermal environments [6], [7]. Faced with these limitations, the electronics industry is turning to more efficient alternatives, in particular the sintering of silver (s-Ag) pastes. This process is emerging as a promising solution thanks to silver's exceptional properties in terms of thermal and electrical conductivity [8], [9], [10]. However, given the industrial constraints requiring an assembly technique at low temperature (below 300°C), at low pressure and time-efficient assembly process, the sintering conditions of the Ag paste result in a porous microstructure, whose evolution over time directly impacts the material's properties.

Most of the studies reported in the literature focus on the macroscopic properties of s-Ag, highlighting their strong dependence on manufacturing parameters [11], [12], [13], [14], [15]. However, these studies rarely establish an explicit link between the material's properties and its microstructural characterization, despite their direct correlation. To analyze the microstructure of s-Ag, two main experimental approaches are commonly employed. The first, 2D characterization using scanning electron microscopy (SEM), provides detailed surface analysis [16], [17], [18], [19], [20]. The second, 3D characterization using X-ray tomography, offers a more comprehensive volumetric exploration, enabling a deeper understanding of the internal structure [21], [22].

After describing the silver sintering process and detailing its key steps, this review article analyzes the porous microstructures obtained after silver sintering based on various approaches. It also examines the impact of thermal aging on the evolution of the material's microstructure. The aim is to highlight the challenges associated with controlling this porous microstructure and to propose perspectives to guide future research.

2. SINTERING PROCESS

The conventional steps involved in the s-Ag die-attach process follow a well-defined sequence. The first stage consists of transforming Ag particles into a paste, a crucial step for its application as a bonding material in electrical systems. This transformation is achieved by mixing Ag powder with organic components, which not only facilitate the formation of the paste but also prevent particle agglomeration and aggregation [9], [23], [24]. Due to the very small size (nanoscale and/or microscale) of the Ag powder used in this technology, two configurations can lead to particle clustering: agglomeration and aggregation. To avoid these, the powder is mixed with specific organic components, namely dispersants, binders, and thinners. Each of these plays a distinct role, enhancing the printability and flowability of the paste [9]. Fig. 1 shows the steps involved in preparing Ag paste [9]. The organic components are first dissolved in an organic solvent to create a uniform solution. Next, the Ag particles, in powder form, are added to the uniform solution while it is being stirred. This stirring ensures the complete and even dispersion of Ag particles within the solution. Finally, to obtain the Ag paste, the organic solvent is evaporated in a controlled process.

Regarding the sintering process itself, there are two main types, primarily depending on the particle size of the Ag. The first is pressure-assisted sintering, which is suitable for microparticles. This method enhances particle adhesion to achieve a material with a low porosity rate [25], [26], [27], [28]. It improves process efficiency and reduces the required sintering temperature but poses challenges in terms of cost and equipment requirements. The second type is pressureless sintering, often used for silver nanoparticles [29], [30], [31]. Regardless of the sintering type, the resulting material remains porous.

Fig. 1: Preparation procedure of nanoscale silver pastes [9], [32].

3. CHARACTERIZATION OF THE 2D POROUS MICROSTRUCTURE OF s-Ag

Most studies on the characterization of the porous microstructure of s-Ag reported in the literature have been conducted in two dimensions (2D) [16], [17], [18], [19]. This section reviews the key works focusing on 2D characterization of the porous structure of silver in its sintered state (i.e., before aging) and its evolution during thermal aging.

a) 2D Microstructure of s-Ag

2D characterization involves surface analysis of the microstructure to estimate certain material properties. Numerous 2D studies have been performed on the microstructure of s-Ag [16], [17], [18], [19]. Fig. 2 shows cross-sectional images obtained by scanning electron microscopy (SEM) from the work of Wakamoto et al., illustrating the microstructure of nano-silver sintered under varying pressures ranging from 5 to 60 MPa at 300 °C for 10 minutes [33]. The porosity of the s-Ag, defined as the ratio of pore area to the total observed area, is indicated alongside each image. Sample preparation conditions play a key role in pore formation. At low pressures of 5 and 10 MPa, the pores exhibit an irregular "peanut" shape and are locally clustered. When the pressure exceeds 30 MPa, the pores become nearly spherical and are evenly distributed. Porosity decreases from 25% at 5 MPa to 14% at 10 MPa, before stabilizing around 5% at pressures of 30 and 60 MPa.

Many studies have reported similar results to those of Wakamoto et al., confirming that higher sintering pressures lead to lower porosity levels. The average pore diameter observed in 2D typically ranges from the nanoscale to a few micrometers, while the porosity of sintered materials varies between 5% and 50%, depending on sintering parameters such as sintering time, temperature, and the type of silver particles used [16], [17], [19], [34], [35], [36], [37].

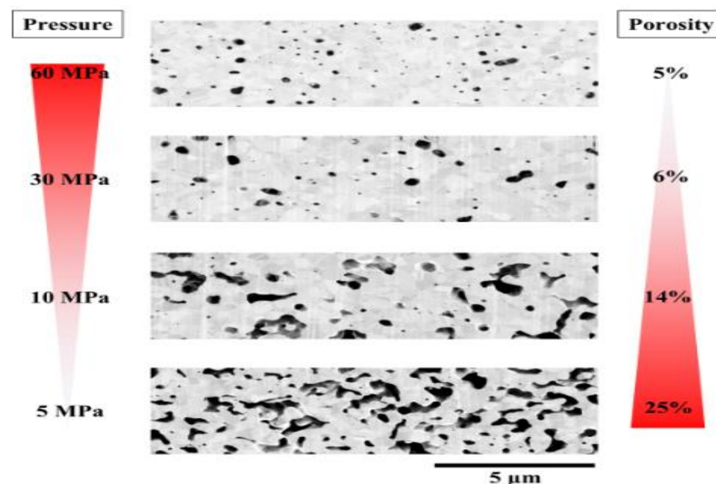

Fig. 2: Cross-sectional SEM images of the nano-silver layer under varying sintering pressures of 5, 10, 30, and 60 MPa at 300 °C for 10 minutes [33], [38].

b) Evolution of the 2D Porous Microstructure in s-Ag

The reliability of s-Ag joints in electronic applications is a critical concern, and it heavily depends on the evolution of their porous microstructure over aging time. This reliability is largely influenced by changes in the pores, a key parameter for understanding the degradation mechanisms of mechanical, thermal, and electrical performance in these joints.

Most studies on the evolution of the porous microstructure during thermal aging reveal a clear trend: the number of pores decreases over time, while their size increases [16], [17], [18], [19], [39]. This phenomenon is

explained by the mechanism of pore coarsening, where smaller pores shrink and disappear, while larger pores continue to grow. Gadaud et al. [18] illustrated this process in Fig. 3, showing SEM images of two samples: one that is unaged and another aged for 1500 hours at 125°C. The unaged sample contains more pores, with an average pore diameter of approximately 80 nm (Fig. 3a), compared to the aged sample with an average diameter of around 150 nm (Fig. 3b).

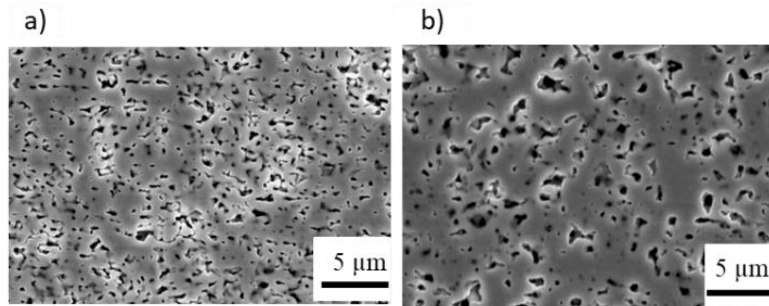

Fig. 3: Porous structure of sintered Ag: a) unaged, b) aged at 125°C for 1500 hours [18].

Table I provides a summary of recent studies comparing the average pore diameters in s-Ag microstructures before and after aging [16], [17], [18]. These studies consistently confirm that pore size systematically increases with aging. Variations in initial average pore diameters at t = 0 across studies are primarily attributed to differences in sample preparation conditions, such as sintering temperature, pressure, and the initial size of the silver particles used in the sintering process.

Table I : Average pore diameters (unaged vs. aged conditions) [16], [17], [18]

Microstructure	Aging Temperature (°C)	Aging Time (h)	Average Pore Diameter (µm)
Microstructure 1 [18]	125	0	0,08
		1500	0,15
Microstructure 2 [17]	250	0	1,59
		1000	1,9
Microstructure 3 [16]	350	0	2
		1200	8

This trend is further confirmed by studies such as those in Fig. 4a and b, which show that as aging time increases, the average pore diameter grows, while the number of pores decreases.

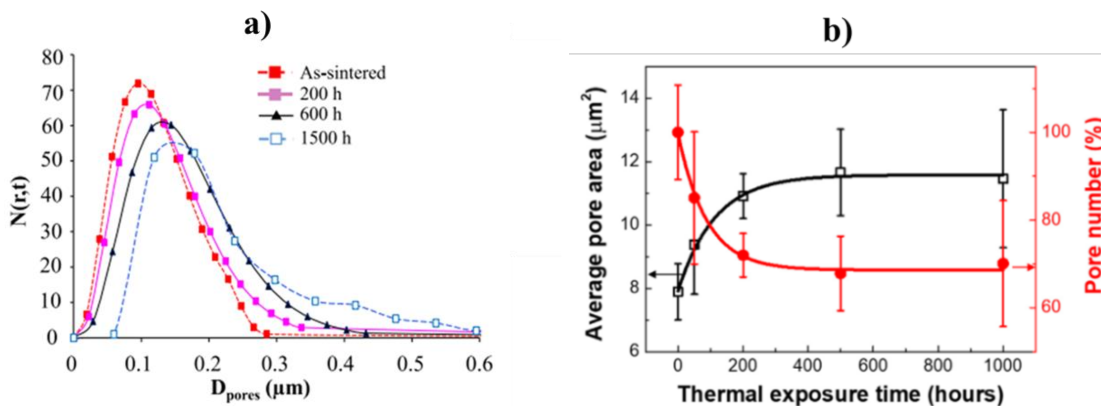

Figure 4: a) Number of pores as a function of diameter for different aging times [18], b) Variation in average pore surface area and number of pores with thermal exposure time [17].

In the work of Gadaud et al. [18], it was demonstrated that the evolution of the average pore diameter in sintered Ag during thermal aging follows the classical thermal evolution law for precipitates, known as Ostwald ripening [40]. In this process, the average diameter of particles (in this case, pores) increases as a function of time and temperature. Ostwald ripening occurs as smaller particles shrink and may even disappear entirely, while larger particles grow. This thermodynamic process is spontaneous, as larger particles are energetically more stable than smaller ones during thermal aging [41].

Numerous studies have also investigated the evolution of material density during thermal aging using 2D characterization methods [16], [17], [18]. The results reported in the literature revealing two main trends. In the first case, random variations in density are observed during thermal aging [16], [17]. In the second case, density remains relatively constant over time [18], [42], [43]. This latter case, where density remains constant, aligns more closely with previously described trends [16], [17], [18], [19], in which the average pore diameter increases while the number of pores decreases, thereby maintaining the overall material density.

c) Influence of the Substrate on the Porous Microstructure

Power electronic modules are composed of multiple components, forming complex networks of interfaces. Several studies have shown that, in the presence of substrates such as Cu, Ag, or Au, phenomena like diffusion, oxidation, and thermal stresses develop within the sintered Ag due to these interfaces [13], [44] (Fig. 5). Recent research has also reported that these interfaces can significantly influence the evolution of the porous structure during thermal aging [16], [19], [44], [45], [46], [47], [48], [49]. However, these studies have not yet provided sufficient data to precisely quantify this effect, which remains critical to the reliability of power modules.

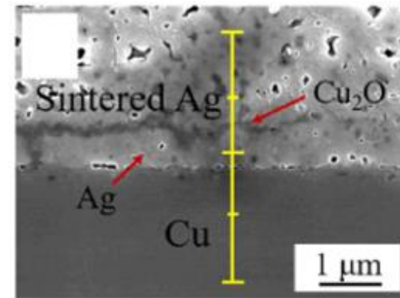

Fig. 5: Oxidation at the Ag/Cu interface [44]

4. CHARACTERIZATION OF THE 3D POROUS STRUCTURE

The 3D characterization of the porous structure of s-Ag is explored in the literature through two main approaches: destructive techniques, which involve serial sectioning under scanning electron microscopy (SEM) [21], [50], [51], and non-destructive techniques, primarily using X-ray tomography [52], [53], [54], [55], [56].

a) 3D Porous Microstructure of s-Ag

Carr et al. [21] conducted a 3D study to characterize the porous structure of sintered silver microparticles. They employed Serial Block Face-Scanning Electron Microscopy (SBF-SEM), a destructive method capable of producing high-resolution 3D images from small samples. Initially developed for brain tissue studies [57], this technique has demonstrated remarkable versatility and can be applied to various sample types. Fig. 6 shows the porous structure observed in their study: interconnected pores, micrometric in size, are shown in red, while isolated pores, submicrometric in size, appear in blue. The silver material (Ag) is rendered transparent for better visualization. Although the study did not provide detailed quantitative data, it highlighted a particularly high connectivity between pores, as suggested by the extensive red regions. This connectivity emphasizes the microstructural heterogeneity, consistent with findings from other studies [21], [50].

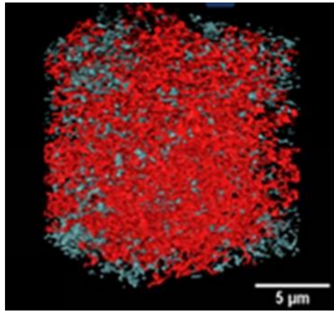

Fig. 6: Porous structure of sintered Ag microparticles in the unaged state [21]

Several studies have employed non-destructive 3D characterization methods based on X-ray tomography [22], [52], [53], [58], [59], highlighting the complexity of the material's structure. Table II summarizes the findings of Zabihzadeh et al. [52], who utilized high-resolution ptychographic X-ray tomography to characterize the 3D microstructure of sintered silver paste under various sintering parameters. The observed microstructures demonstrate a clear dependency on sintering conditions. Across all configurations, more than 90% of the porous volume was interconnected, while isolated pores accounted for only a small fraction of the total porous volume. These results corroborate findings from SBF-SEM studies. Similar observations have been reported in other studies [53], [58], further validating these trends.

Table II : Porosity rates and pore connectivity as a function of sintering parameters [52]

Sample	Température (°C)	Pressure (MPa)	Sintering duration (min)	Porosity (%)	Pore Connectivity (%)
S1	210	4	3	47	**99,4**
S2	250	4	10	45	**99**
S4	250	8	3	41	**99**
S4	300	8	3	35	**98**
S5	250	8	10	29	**98**
S6	210	12	10	33	**97**
S7	250	12	10	32	**97**
S8	300	12	10	22	**91**

A detailed investigation into the 3D nanoporous structure of several sintered silver samples, conducted via X-ray nanotomography, revealed that the pore population can be divided into two distinct categories [22]. The first category comprises the majority of pores, whose equivalent diameter distribution appears to follow a log-normal law, with an average size of a few hundred nanometers (Fig. 7a). The second category consists of a few highly complex pores, with equivalent diameters reaching several micrometers (Fig. 7b). In Fig. 7a and b, 494 small pores (SP) belong to the first category, while only one large pore (LP) is classified in the second. These findings align with studies demonstrating that more than 90% of the porous volume is interconnected [52].

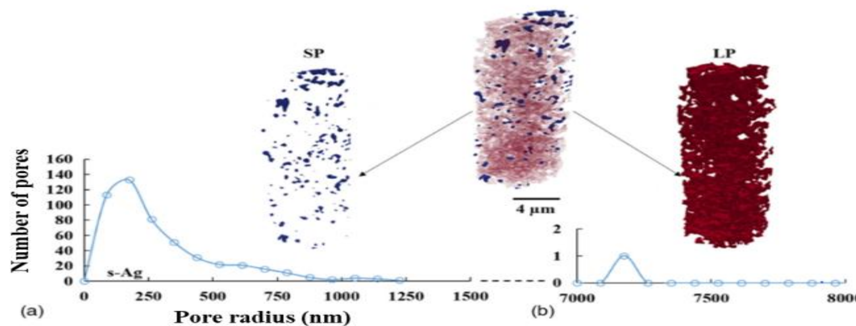

Fig. 7: Pore distribution within the volume of an as-processed Ag pillar consisting of two groups based on their radius: a) Size distribution of the numerous isolated small pores (SP - in blue on the tomogram) vs b) 1 very large pore (LP - in red [22])

b) Evolution of the 3D porous microstructure of s-Ag during thermal aging

The temporal evolution of the 3D porous structure in s-Ag has been extensively studied to gain insights into its behavior during thermal aging. Milhet et al. [53], using X-ray nanotomography, investigated the 3D porous structure of s-Ag across a temperature range of 180°C to 300°C. Their findings indicate that, while the material's density remains constant, its microstructure undergoes significant changes over time. Specifically, the average pore volume increases with both aging time and temperature, aligning with trends reported in 2D studies [16], [17], [18]. This evolution in 3D also follows the classical Ostwald ripening mechanism, where smaller pores shrink and larger pores grow.

To explore the evolution of s-Ag in conditions closer to practical applications, N'tsouaglo et al. examined s-Ag samples, both coated with copper and uncoated, subjected to thermal aging at temperatures between 200°C and 350°C [22]. This study emphasized the role of copper interfaces, commonly used in real-world power modules, on the porous structure's evolution. Their results showed a noticeable increase in structural complexity during aging, although the material's density remained relatively stable for both coated and uncoated samples (Fig. 8a). However, significant differences were observed between the two types of samples (Fig. 8b). For uncoated samples, the pore evolution was characterized by Ostwald ripening: the average pore volume increased linearly with time as the number of pores decreased. In contrast, coated samples exhibited more complex behavior, with the average pore volume initially increasing up to a critical time point before deviations appeared (Fig 8b). This deviation was attributed to thermally induced stresses caused by the mismatch in thermal expansion coefficients between copper and silver, which gradually relaxed during aging. The presence of copper was found to accelerate the evolution of the porous structure.

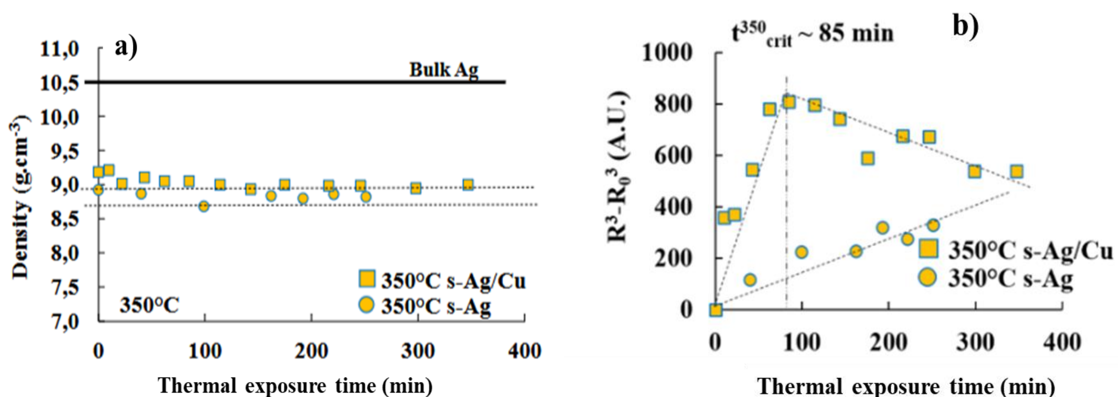

Figure 8: a) Evolution of density versus aging time at 350°C for s-Ag and s-Ag/Cu, b) Average pore radius evolution versus aging time for s-Ag and s-Ag/Cu at 350°C [22].

Further analysis by N'tsouaglo et al. [22] focused on categorizing the pores into two populations: small pores and large pores. They observed that the volume of small pores remained relatively constant during thermal aging, whereas the evolution of the porous structure was predominantly driven by the large pores. These results suggest that controlling the overall evolution of the porous structure in s-Ag paste hinges on effectively managing the large pores networks, which can sometimes span the entire volume of the samples. However, it should be noted that the experiments carried out on the evolution of the 3D microstructure were not conducted over a long period of time (around 7 hours). This constraint restricts the conclusions that can

be drawn about the long-term evolution of the microstructure, particularly in the presence of a coating.

5. COMPARATIVE ANALYSIS: 2D VS 3D MICROSTRUCTURAL CHARACTERIZATION

The reported results on the evolution of the density of s-Ag vary depending on whether 2D or 3D approaches were used for the study. In 2D, some studies report a variation in density during thermal aging [16], [17], [39], while others observe no densification at all [18], [42], [60]. In contrast, 3D studies consistently show that density remains nearly stable throughout aging. It is important to note that studies showing a variation in density during aging are generally based on changes in pore surface fraction. For instance, Choe et al [17], concluded that densification occurred during aging in their 2D study, as shown in Fig. 4b. However, by multiplying the average pore surface area by the number of pores reported in their figure, the results in Table III reveal that the surface porosity fraction remains almost constant over time. This result contradicts their conclusion of densification, shows the limitations of surface analysis, which can be misleading and is sensitive to the size and distribution of the pores within the selected analysis window.

Table III : Review of results from choe et al. [17]

Aging time (hours)	0	50	200	500	1000
Average pore surface (µm^2)	7.9	9.3	10.8	11.5	11.3
Number of pores (%)	100	85	73	69	70
Surface porosity (µm²)	**790**	**790.5**	**788.4**	**793.5**	**791**

The differences observed between 2D and 3D studies result mainly from the impossibility of taking into account the interconnectivity of pores in a 2D analysis. In 2D, large pores often appear as distinct small pores, unlike in 3D, where interconnectivity is accurately captured [22], [52]. For example, a study by N'Tsouaglo [59] performed both 3D and 2D analyses on a cubic volume (5.6 × 5.6 × 5.6 µm³) of a s-Ag sample. Fig. 9 shows this 3D volume, where porosity is shown in blue and silver is rendered transparent. A surface cross-section (corresponding to the red plane) shows the pores in white and silver in black. At t = 85 minutes during thermal aging at 350°C, the 3D analysis revealed a single pore with an equivalent radius of 1.35 µm (Fig. 9a). At t = 216 minutes, the same pore grew to a radius of 1.41 µm (Fig. 9b). However, the 2D analysis misinterpreted the data, indicating multiple smaller pores with average radii increasing from 0.30 µm to 0.33 µm during thermal aging. In summary, 2D analyses can lead to incorrect interpretations of microstructural evolution by failing to account for pore interconnectivity. In contrast, 3D approaches provide a more accurate and consistent understanding of the actual densification behavior of s-Ag samples during aging, though they require significant resources.

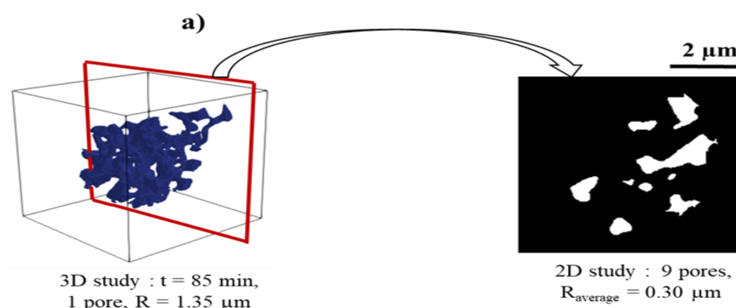

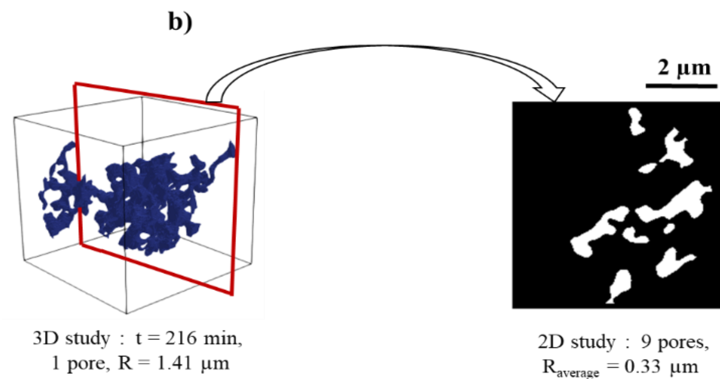

Fig. 9: Comparison of 3D and 2D studies.

6. CONCLUSION

This review on the characterization of the porous structures of sintered silver and their evolution during thermal aging aims to understand the impact of aging on the microstructure, an essential factor for evaluating its reliability as a promising solution for electronic component assemblies.

Many studies focus mainly on 2D analyses using SEM, showing that pores are nanometric and/or micrometric in size. While these observations provide valuable insights into nanoporous microstructure characterization (e.g., pore surface area, number, and size), the 2D approach is limited by its inability to capture pore interconnectivity, a critical factor in understanding structural evolution during thermal aging. Moreover, tracking the same area on a sample over time is rarely achievable in 2D. In contrast, 3D studies provide a more comprehensive perspective, allowing in situ tracking of the porous structure's evolution, but require more resources. Under these conditions, studies of sintered silver's porous structure indicate that overall density remains constant despite a reduction in the number of pores and an increase in their average size. Additionally, 3D analyses identify two categories of pores: the first, comprising the majority (small pores), follows a log-normal distribution with equivalent diameters of a few hundred nanometers, while the second (large pores), much rarer, has diameters of several micrometers. Large pores appear to play a central role in microstructural evolution, suggesting that controlling these pore networks may be key to managing the porous structure of sintered silver.

Furthermore, both 2D and 3D analyses reveal that the presence of a substrate interface induces phenomena such as diffusion, oxidation, and thermal stresses, which significantly influence the evolution of the porous structure during thermal aging. However, current data remain insufficient to precisely quantify these effects.

For future research, more detailed 3D studies conducted over long aging times (beyond 7 hours) are recommended. These studies should focus on the impact of the sintered Ag/substrate interface on microstructural evolution. Long-term investigations could track pore evolution, explore changes in the roughness of the sintered Ag/substrate interface during thermal aging, and provide deeper insights into the mechanisms occurring at interfaces under real-world operating conditions.

Declaration by Authors

Acknowledgement: None
Source of Funding: None
Conflict of Interest: No conflicts of interest declared.

REFERENCES

1. L. F. S. Alves, P. Lefranc, P.-O. Jeannin, et B. Sarrazin, « Review on SiC-MOSFET devices and associated gate drivers », in *2018 IEEE International Conference on Industrial Technology (ICIT)*, févr. 2018, p. 824-829. doi: 10.1109/ICIT.2018.8352284.

2. J. Biela, M. Schweizer, S. Waffler, et J. W. Kolar, « SiC versus Si—Evaluation of Potentials for Performance Improvement of Inverter and DC–DC Converter Systems by SiC Power Semiconductors », *IEEE Trans. Ind. Electron.*, vol. 58, nº 7, p. 2872-2882, juill. 2011, doi: 10.1109/TIE.2010.2072896.
3. A. Turner et M. Filella, « Lead in plastics – Recycling of legacy material and appropriateness of current regulations », *J. Hazard. Mater.*, vol. 404, p. 124131, févr. 2021, doi: 10.1016/j.jhazmat.2020.124131.
4. N. Alayli, A. Girard, F. Schoenstein, P.-R. Dahoo, K. L. Tan, et J. M. Morelle, « Etude du frittage de particules d'argent pour la connexion dans un système électronique de puissance », *Matér. 2010*, p. 9, 2010.
5. S. Menon, E. George, M. Osterman, et M. Pecht, « High lead solder (over 85 %) solder in the electronics industry: RoHS exemptions and alternatives », *J. Mater. Sci. Mater. Electron.*, vol. 26, nº 6, p. 4021-4030, juin 2015, doi: 10.1007/s10854-015-2940-4.
6. H. Yan, P. Liang, Y. Mei, et Z. Feng, « Brief review of silver sinter-bonding processing for packaging high-temperature power devices », *Chin. J. Electr. Eng.*, vol. 6, nº 3, p. 25-34, sept. 2020, doi: 10.23919/CJEE.2020.000016.
7. B. Boursat, « Comprendre les problèmes de procédé de l'électronique de puissance. », *Présentation Alstom PEARL*, janvier 2006.
8. K. S. Siow, « Are Sintered Silver Joints Ready for Use as Interconnect Material in Microelectronic Packaging? », *J. Electron. Mater.*, vol. 43, nº 4, p. 947-961, avr. 2014, doi: 10.1007/s11664-013-2967-3.
9. G. Bai, « Low-Temperature Sintering of Nanoscale Silver Paste for Semiconductor Device Interconnection », *Ph.D. dissertation, Virginia Polytechnic Institute and State University, oct. 2005.*
10. V. R. Manikam et K. Y. Cheong, « Die Attach Materials for High Temperature Applications: A Review », *IEEE Trans. Compon. Packag. Manuf. Technol.*, vol. 1, nº 4, p. 457-478, avr. 2011, doi: 10.1109/TCPMT.2010.2100432.
11. K. S. Siow, « Mechanical properties of nano-silver joints as die attach materials », *J. Alloys Compd.*, vol. 514, p. 6-19, févr. 2012, doi: 10.1016/j.jallcom.2011.10.092.
12. R. Khazaka, L. Mendizabal, et D. Henry, « Review on Joint Shear Strength of Nano-Silver Paste and Its Long-Term High Temperature Reliability », *J. Electron. Mater.*, vol. 43, nº 7, p. 2459-2466, juill. 2014, doi: 10.1007/s11664-014-3202-6.
13. X. Milhet, P. Gadaud, V. Caccuri, D. Bertheau, D. Mellier, et M. Gerland, « Influence of the Porous Microstructure on the Elastic Properties of Sintered Ag Paste as Replacement Material for Die Attachment », *J. Electron. Mater.*, vol. 44, nº 10, p. 3948-3956, oct. 2015, doi: 10.1007/s11664-015-3791-8.
14. G. Zou, J. Yan, F. Mu, A. Wu, J. Ren, et A. Hu, « Low Temperature Bonding of Cu Metal through Sintering of Ag Nanoparticles for High Temperature Electronic Application », *Open Surf. Sci. J.*, vol. 3, nº 1, mai 2011
15. L. A. Navarro *et al.*, « Thermomechanical Assessment of Die-Attach Materials for Wide Bandgap Semiconductor Devices and Harsh Environment Applications », *IEEE Trans. Power Electron.*, vol. 29, nº 5, p. 2261-2271, mai 2014, doi: 10.1109/TPEL.2013.2279607.
16. H. Zhang *et al.*, « Microstructural and mechanical evolution of silver sintering die attach for SiC power devices during high temperature applications », *J. Alloys Compd.*, vol. 774, p. 487-494, févr. 2019, doi: 10.1016/j.jallcom.2018.10.067.
17. C. Choe, S. Noh, C. Chen, D. Kim, et K. Suganuma, « Influence of thermal exposure upon mechanical/electrical properties and microstructure of sintered micro-porous silver », *Microelectron. Reliab.*, vol. 88-90, p. 695-700, sept. 2018, doi: 10.1016/j.microrel.2018.07.048.
18. P. Gadaud, V. Caccuri, D. Bertheau, J. Carr, et X. Milhet, « Ageing sintered silver: Relationship between tensile behavior, mechanical properties and the nanoporous structure evolution », *Mater. Sci. Eng. A*, vol. 669, p. 379-386, juill. 2016, doi: 10.1016/j.msea.2016.05.108.
19. S. A. Paknejad, G. Dumas, G. West, G. Lewis, et S. H. Mannan, « Microstructure evolution during 300°C storage of sintered Ag nanoparticles on Ag and Au substrates », *J. Alloys Compd.*, vol. 617, p. 994-1001, déc. 2014, doi: 10.1016/j.jallcom.2014.08.062.
20. S. A. Paknejad, A. Mansourian, J. Greenberg, K. Khtatba, L. Van Parijs, et S. H. Mannan, « Microstructural evolution of

sintered silver at elevated temperatures », *Microelectron. Reliab.*, vol. 63, p. 125-133, août 2016, doi: 10.1016/j.microrel.2016.06.007.

21. J. Carr, X. Milhet, P. Gadaud, S. A. E. Boyer, G. E. Thompson, et P. Lee, « Quantitative characterization of porosity and determination of elastic modulus for sintered micro-silver joints », *J. Mater. Process. Technol.*, vol. 225, p. 19-23, nov. 2015, doi: 10.1016/j.jmatprotec.2015.03.037.
22. K. H. N'Tsouaglo *et al.*, « Time-Resolved Evolution of the 3D Nanoporous Structure of Sintered Ag by X-Ray Nanotomography: Role of the Interface with a Copper Substrate », *Adv. Eng. Mater.*, vol. 24, nº 1, p. 2100583, 2022, doi: 10.1002/adem.202100583.
23. S. M. Heard, F. Grieser, C. G. Barraclough, et J. V. Sanders, « The characterization of ag sols by electron microscopy, optical absorption, and electrophoresis », *J. Colloid Interface Sci.*, vol. 93, nº 2, p. 545-555, juin 1983, doi: 10.1016/0021-9797(83)90439-3.
24. V. Caccuri, « Etude des propriétés mécaniques de technologies de report de puce pour électronique de puissance : influence du vieillissement. », phdthesis, ISAE-ENSMA Ecole Nationale Supérieure de Mécanique et d'Aérotechique - Poitiers, 2014. Consulté le: 1 mars 2021. [En ligne]. Disponible sur: https://tel.archives-ouvertes.fr/tel-01196618
25. Z. Zhang et G.-Q. Lu, « Pressure-assisted low-temperature sintering of silver paste as an alternative die-attach solution to solder reflow », *IEEE Trans. Electron. Packag. Manuf.*, vol. 25, nº 4, p. 279-283, oct. 2002, doi: 10.1109/TEPM.2002.807719.
26. Y. Liu, H. Zhang, L. Wang, X. Fan, G. Zhang, et F. Sun, « Stress analysis of pressure-assisted sintering for the double-side assembly of power module », *Solder. Surf. Mt. Technol.*, vol. 31, nº 1, p. 20-27, janv. 2019, doi: 10.1108/SSMT-01-2018-0005.
27. S. A. Paknejad et S. H. Mannan, « Review of silver nanoparticle based die attach materials for high power/temperature applications », *Microelectron. Reliab.*, vol. 70, p. 1-11, mars 2017, doi: 10.1016/j.microrel.2017.01.010.
28. Y. Liu, H. Zhang, L. Wang, X. Fan, G. Zhang, et F. Sun, « Effect of Sintering Pressure on the Porosity and the Shear Strength of the Pressure-Assisted Silver Sintering Bonding », *IEEE Trans. Device Mater. Reliab.*, vol. 18, nº 2, p. 240-246, juin 2018, doi: 10.1109/TDMR.2018.2819431.
29. N. Heuck, G. Palm, T. Sauerberg, A. Stranz, A. Waag, et A. Bakin, « SiC-Die-Attachment for High Temperature Applications », *Mater. Sci. Forum*, vol. 645-648, p. 741-744, 2010, doi: 10.4028/www.scientific.net/MSF.645-648.741.
30. X. Long, W. Tang, W. Xia, Y. Wu, L. Ren, et Y. Yao, « Porosity and Young's modulus of pressure-less sintered silver nanoparticles », in *2017 IEEE 19th Electronics Packaging Technology Conference (EPTC)*, déc. 2017, p. 1-8. doi: 10.1109/EPTC.2017.8277577.
31. M. Wang, Y. Mei, X. Li, R. Burgos, D. Boroyevich, et G.-Q. Lu, « Pressureless Silver Sintering on Nickel for Power Module Packaging », *IEEE Trans. Power Electron.*, vol. 34, nº 8, p. 7121-7125, août 2019, doi: 10.1109/TPEL.2019.2893238.
32. J. G. Bai, J. N. Calata, et G.-Q. Lu, « Processing and Characterization of Nanosilver Pastes for Die-Attaching SiC Devices », *IEEE Trans. Electron. Packag. Manuf.*, vol. 30, nº 4, p. 241-245, oct. 2007, doi: 10.1109/TEPM.2007.906508.
33. K. Wakamoto, Y. Mochizuki, T. Otsuka, K. Nakahara, et T. Namazu, « Tensile mechanical properties of sintered porous silver films and their dependence on porosity », *Jpn. J. Appl. Phys.*, vol. 58, nº SD, p. SDDL08, mai 2019, doi: 10.7567/1347-4065/ab0491.
34. P. Gadaud, V. Caccuri, D. Bertheau, J. Carr, et X. Milhet, « Ageing sintered silver: Relationship between tensile behavior, mechanical properties and the nanoporous structure evolution », *Mater. Sci. Eng. A*, vol. 669, p. 379-386, juill. 2016, doi: 10.1016/j.msea.2016.05.108.
35. S. T. Chua et K. S. Siow, « Microstructural studies and bonding strength of pressureless sintered nano-silver joints on silver, direct bond copper (DBC) and copper substrates aged at 300 °C », *J. Alloys Compd.*, vol. 687, p. 486-498, déc. 2016, doi: 10.1016/j.jallcom.2016.06.132.
36. M. Calabretta, A. Sitta, S. M. Oliveri, et G. Sequenzia, « Silver Sintering for Silicon

Carbide Die Attach: Process Optimization and Structural Modeling », *Appl. Sci.*, vol. 11, nº 15, Art. nº 15, janv. 2021, doi: 10.3390/app11157012.

37. G. F. BOCCHINI, « The influence of porosity on the characteristics of sintered materials », *Influ. Porosity Charact. Sintered Mater.*, vol. 22, nº 3, p. 185-202, 1986.
38. K. Wakamoto et T. Namazu, « Mechanical Characterization of Sintered Silver Materials for Power Device Packaging: A Review », *Energies*, vol. 17, nº 16, Art. nº 16, janv. 2024, doi: 10.3390/en17164105.
39. J. Dai, J. Li, P. Agyakwa, M. Corfield, et C. M. Johnson, « Comparative Thermal and Structural Characterization of Sintered Nano-Silver and High-Lead Solder Die Attachments During Power Cycling », *IEEE Trans. Device Mater. Reliab.*, vol. 18, nº 2, p. 256-265, juin 2018, doi: 10.1109/TDMR.2018.2825386.
40. I. M. Lifshitz et V. V. Slyozov, « The kinetics of precipitation from supersaturated solid solutions », *J. Phys. Chem. Solids*, vol. 19, nº 1, p. 35-50, avr. 1961, doi: 10.1016/0022-3697(61)90054-3.
41. L. Ratke et P. W. Voorhees, *Growth and Coarsening: Ostwald Ripening in Material Processing*. in Engineering Materials. Berlin Heidelberg: Springer-Verlag, 2002. doi: 10.1007/978-3-662-04884-9.
42. F. Yu, R. W. Johnson, et M. Hamilton, « Pressureless, Low Temperature Sintering of Micro-scale Silver Paste for Die Attach for 300°C Applications », *Addit. Conf. Device Packag. HiTEC HiTEN CICMT*, vol. 2014, nº HITEC, p. 000165-000171, janv. 2014, doi: 10.4071/HITEC-WA21.
43. R. Dou, B. Xu, et B. Derby, « High-strength nanoporous silver produced by inkjet printing », *Scr. Mater.*, vol. 63, nº 3, p. 308-311, août 2010, doi: 10.1016/j.scriptamat.2010.04.021.
44. F. Yang, W. Zhu, W. Wu, H. Ji, C. Hang, et M. Li, « Microstructural evolution and degradation mechanism of SiC–Cu chip attachment using sintered nano-Ag paste during high-temperature ageing », *J. Alloys Compd.*, vol. 846, p. 156442, déc. 2020, doi: 10.1016/j.jallcom.2020.156442.
45. Y.-C. Lin *et al.*, « Unveiling 3D Morphology of Multiscale Micro-Nanosilver Sintering for Advanced Electronics Manufacturing by Ptychographic X-ray Nanotomography », *Adv. Eng. Mater.*, vol. 22, nº 4, p. 1901250, 2020, doi: 10.1002/adem.201901250.
46. I. L. Regalado, J. J. Williams, S. Joshi, E. M. Dede, Y. Liu, et N. Chawla, « X-Ray Microtomography of Thermal Cycling Damage in Sintered Nano-Silver Solder Joints », *Adv. Eng. Mater.*, vol. 21, nº 3, p. 1801029, 2019, doi: 10.1002/adem.201801029.
47. P. Agyakwa *et al.*, « Three-dimensional damage morphologies of thermomechanically deformed sintered nanosilver die attachments for power electronics modules », *J. Microsc.*, vol. 277, nº 3, p. 140-153, 2020, doi: 10.1111/jmi.12803.
48. W. Xiaoting, J. He, Z. Peng, Y. Fan, et Z. Wenbo, « High-Temperature Reliability of Nano-Ag Sintered Joints on Ag-Plated Cu Substrates », *J. Phys. Conf. Ser.*, vol. 2690, nº 1, p. 012009, janv. 2024, doi: 10.1088/1742-6596/2690/1/012009.
49. P. A. Agyakwa *et al.*, « Microstructural Response of Highly Porous Sintered Nano-silver Particle Die Attachments to Thermomechanical Cycling », *J. Electron. Mater.*, vol. 53, nº 3, p. 1374-1398, mars 2024, doi: 10.1007/s11664-023-10870-4.
50. T. Youssef *et al.*, « Power modules die attach: A comprehensive evolution of the nanosilver sintering physical properties versus its porosity », *Microelectron. Reliab.*, vol. 55, nº 9, p. 1997-2002, août 2015, doi: 10.1016/j.microrel.2015.06.085.
51. M. Ziehmer, K. Hu, K. Wang, et E. T. Lilleodden, « A principle curvatures analysis of the isothermal evolution of nanoporous gold: Quantifying the characteristic length-scales », *Acta Mater.*, vol. 120, p. 24-31, nov. 2016, doi: 10.1016/j.actamat.2016.08.028.
52. S. Zabihzadeh, S. Van Petegem, M. Holler, A. Diaz, L. I. Duarte, et H. Van Swygenhoven, « Deformation behavior of nanoporous polycrystalline silver. Part I: Microstructure and mechanical properties », *Acta Mater.*, vol. 131, p. 467-474, juin 2017, doi: 10.1016/j.actamat.2017.04.021.
53. X. Milhet *et al.*, « Evolution of the nanoporous microstructure of sintered Ag at high temperature using in-situ X-ray nanotomography », *Acta Mater.*, vol. 156, p. 310-317, sept. 2018, doi: 10.1016/j.actamat.2018.06.047.

54. Y. K. Chen-Wiegart *et al.*, « Structural evolution of nanoporous gold during thermal coarsening », *Acta Mater.*, vol. 60, nº 12, p. 4972-4981, juill. 2012, doi: 10.1016/j.actamat.2012.05.012.
55. A. J. Shahani, X. Xiao, E. M. Lauridsen, et P. W. Voorhees, « Characterization of metals in four dimensions », *Mater. Res. Lett.*, vol. 8, nº 12, p. 462-476, déc. 2020, doi: 10.1080/21663831.2020.1809544.
56. L. Wang *et al.*, « Influence of pores on crack initiation in monotonic tensile and cyclic loadings in lost foam casting A319 alloy by using 3D in-situ analysis », *Mater. Sci. Eng. A*, vol. 673, p. 362-372, sept. 2016, doi: 10.1016/j.msea.2016.07.036.
57. W. Denk et H. Horstmann, « Serial Block-Face Scanning Electron Microscopy to Reconstruct Three-Dimensional Tissue Nanostructure », *PLOS Biol.*, vol. 2, nº 11, p. e329, oct. 2004, doi: 10.1371/journal.pbio.0020329.
58. W. Rmili, N. Vivet, S. Chupin, T. Le Bihan, G. Le Quilliec, et C. Richard, « Quantitative Analysis of Porosity and Transport Properties by FIB-SEM 3D Imaging of a Solder Based Sintered Silver for a New Microelectronic Component », *J. Electron. Mater.*, vol. 45, nº 4, p. 2242-2251, avr. 2016, doi: 10.1007/s11664-015-4288-1.
59. K. H. N'Tsouaglo, « Vieillissement thermique de la structure nanoporeuse de l'Ag fritté pour le report de puces des modules d'électronique de puissance : nanotomographie in situ, rôle d'une interface et simulation du comportement mécanique », Ph.D. dissertation, ISAE-ENSMA Ecole Nationale Supérieure de Mécanique et d'Aérotechique - Poitiers, 2022. [online]. Available: https://theses.hal.science/tel-03813616
60. R. Dou, B. Xu, et B. Derby, « High-strength nanoporous silver produced by inkjet printing », *Scr. Mater.*, vol. 63, nº 3, p. 308-311, août 2010, doi: 10.1016/j.scriptamat.2010.04.021.

How to cite this article: Kokouvi Happy N'TSOUAGLO, Komlavi GOGOLI, Kodjo ATTIPOU. Comprehensive review of sintered silver porous structures and their thermal aging for power device packaging. *International Journal of Research and Review*. 2025; 12(3): 174-186. DOI: *10.52403/ijrr.20250325*

******